Weld World (2017) 61:603–611
DOI 10.1007/s40194-017-0445-x

RESEARCH PAPER

Study of intermetallic compounds (IMC) that form between indium-enriched SAC solder alloys and copper substrate

Felipe Rodrigues[1] · **Jonathan Watson**[1] · **Stephen Liu**[1] · **Juan C. Madeni**[1]

Received: 26 August 2016 / Accepted: 11 February 2017 / Published online: 7 March 2017

Abstract This paper evaluates the characteristics of the intermetallic compounds (IMC) that form between Indium-enriched SAC solder alloys and Copper substrate. In this study, Indium was added to a commercial SAC305 solder (96.5 wt.% Sn, 3 wt.% Ag, 0.5 wt.% Cu) at three different compositions, 0.5, 5, and 10 wt%. To observe IMC growth during the liquid state of the solder droplet, the experimental matrix consisted in three soldering temperatures (220, 275, and 300 °C), and the molten solder was kept at this temperature for 2, 5, and 8 s. Fast cooling followed each solder test to complete solidification. The same procedure was repeated for the three levels of Indium. The Copper substrate/solder alloy interface was examined using light microscopy, scanning electron microscopy, and energy dispersive spectroscopy. Statistical analysis was performed on the IMC thickness data obtained from the long profile analyses. Using Arrhenius analysis, the activation energy for IMC formation and growth was calculated to be approximately 6.7, 5.1, and 10.8 kCal/mol for the SAC305 alloys with 0.5, 5.0, and 10 wt% Indium additions, respectively. As expected, Cu_6Sn_5, Cu_3Sn, Ag_3Sn, In_3Sn (β), $InSn_4$ (γ), and $AgIn_2$ were observed.

Keywords (IIW thesaurus) Lead free solders · Indium · Intermetallics

Recommended for publication by Commission XVII-Brazing, Soldering and Diffusion Bonding

✉ Stephen Liu
sliu@mines.edu

[1] Center for Welding, Joining and Coatings Research, Colorado School of Mines, Golden, CO 80401, USA

1 Introduction

Due to new environmental, health and safety regulations, the use of lead has been reduced or prohibited in many countries [1]. Alternative materials have been sought in the development of lead-free solders for industrial applications [2, 3]. Materials such as antimony, bismuth, copper, indium, silver, or zinc have been investigated [4]. The most widely used lead-free solder is the SAC family (Sn–Ag–Cu) [5]. Indium and Iron alloying additions to SAC alloys have been shown to improve the fracture toughness and shear strength of the solder joints, but can also lead to the formation of brittle intermetallic compounds at the solder substrate interface [6]. Indium additions in the range of 20–100 wt.% have also been investigated for use soldering Ti alloys [7]. It is desirable to investigate the effects that Indium has on intermetallic formation at the solder-substrate interface in these alloys.

In this study, the effects of Indium addition in the commercial SAC305 alloy (Sn-3.0 wt%Ag–0.5 wt%Cu) were studied. Pure Indium was added to commercial SAC305 solder to obtain alloys with 0.5, 5.0, and 10 wt% Indium. The different intermetallic compounds formed in the interface between the solder and the Copper substrate were characterized. The activation energies for the formation of the IMC's under the different soldering conditions have also been calculated and compared with those found for the SAC alloys [8].

Experimental setup and parameters were selected to specifically investigate intermetallic compound growth along the solder/substrate interface while the solder droplet was in the molten state and during solidification. Since the presence of an IMC layer is generally linked to deteriorated qualities of a solder [9–12], understanding the intermetallic compound layer growth rate, activation

energy, and extent of growth during solidification is critical to the design of a new solder alloy and the selection of optimal operating parameters (time and temperature of soldering) for minimizing IMC formation [8, 13].

2 Experimental procedure

In this series of experiments, three laboratory solder compositions were tested on a Copper substrate. Three temperatures (220, 275, and 300 °C) were chosen, initially based on the Cu–Sn equilibrium binary phase diagram [14]. The heat was applied for three times (2, 5, and 8 s after the solder was melted). After the predetermined hold time, the heat source was removed for faster cooling and solidification of the molten solder droplet.

The solder alloys used in this study were made in the laboratory using the commercial SAC305 alloy as the base material. Pure Indium was melted with the commercial solder in an argon atmosphere furnace to obtain the experimental alloys with 0.5, 5.0, and 10 wt.% of Indium. The experimental alloys were rolled, ground with No.600 grit paper and ultrasonically cleaned to remove any visible oxides from the surface. The compositions of the alloys were verified in three different positions on the samples with X-Ray fluorescence, as shown in Table 1.

Copper coupons of 25.4 × 12.7 × 0.8 mm were annealed at 650 °C for 20 min to remove residual stresses and ground with No.800 grit paper to achieve an oxidation-free surface. Ultrasonic cleaning and a final cleaning/drying step with isopropanol were performed just before soldering to ensure a particle-free surface.

The as-rolled solder foils were cut to produce 0.1 g solder samples. Before the heat was applied to the substrate, a layer of commercial lead-free solder flux was applied to the coupon, to protect the surface from oxidation and to remove any oxide that form during the heating process.

As indicated earlier, three soldering temperatures, T_1 = 220 °C, T_2 = 275 °C and T_3 = 300 °C were selected to investigate the intermetallic compound layer formation during solidification. T_1 is just below the Sn–Cu eutectic temperature of 227 °C [14] and above the melting range of the SAC305 alloy, between 217 and 220 °C [15]. T_2 is reported to be the temperature of formation of Cu_6Sn_5 and T_3, a higher temperature that ensures the formation of Cu_6Sn_5.

Each level of the experimental matrix also included three times of soldering, 2, 5, and 8 s. In this paper, the soldering time is defined as the time interval when the solder droplet is molten, i.e., from the moment of melting the solder till when the heat source is removed (for the onset of solidification). Combining time and temperature, nine different soldering conditions were defined for each composition, resulting in a total of 27 samples.

During the test, the solder gun was placed immediately below and in contact with the bottom side of the copper substrate; the temperature was kept constant at the predetermined level. The solder piece was placed on the copper substrate, and the temperature was measured with a thermocouple and placed immediately outside the solder position. After the predetermined time, the heat gun was removed to allow for cooling and solidification.

Metallographic preparation was carefully conducted to avoid heating up of the samples which could promote changes in the intermetallic compound layer. Each sample was cut using a low speed cutting machine and cold mounted using epoxy. Grinding and diamond polishing followed by 1 hour Vibromet polishing using 0.04 μm colloidal silica were performed. Microstructural characterization of the samples was made using light and electron microscopy (ESEM and FESEM); elemental characterization was made using energy dispersive spectroscopy (EDS).

Optical micrographs were taken for all the 27 samples at 500 or 1000 magnification. Ten photomicrographs were taken for each sample, covering between 500 to 1200 μm of distance along the interface on each sample. Intermetallic compound layer thickness was measured at 10 μm intervals using the ImageJ software.

Table 1 XRF composition of the experimental solder alloys

	0% In (Nominal)		0.5% In (Nominal)		5% In (Nominal)		10% In (Nominal)	
	Composition (wt.%)	Variance along the sample (wt.%)	Composition (wt.%)	Variance along the sample (wt.%)	Composition (wt.%)	Variance along the sample (wt.%)	Composition (wt.%)	Variance along the sample (wt.%)
In	0.00	0.00	0.41	0.02	4.51	0.25	9.98	0.06
Sn	96.51	0.39	96.12	0.09	92.23	0.30	86.98	0.54
Ag	2.96	0.21	2.94	0.06	2.80	0.03	2.62	0.00
Cu	0.53	0.02	0.53	0.08	0.46	0.02	0.42	0.00
Sum	100		100		100		100	

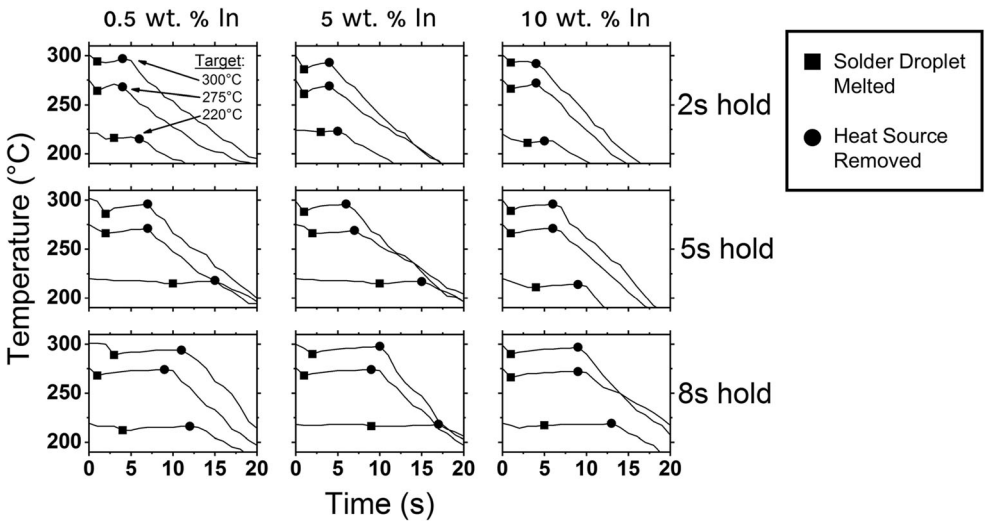

Fig. 1 Time temperature profiles for each solder alloy and test condition. The same *x* and *y* scale was used for all the plots

3 Results and discussion

The results obtained in this study included IMC layer thickness, IMC formation, and growth activation energy and IMC composition. Time-temperature profiles of the soldering tests to demonstrate that correct heating and cooling conditions were followed during the tests are presented in Fig. 1. The hold time is fixed in each row, and the alloy is fixed in each column. In each plot, target temperatures of 220, 275, and 300 °C are shown. On each T-*t* plot, the square marks the time when the solder droplet became molten, and the circle marks the time that the heat source was removed.

The fast cooling rate after the removal of the heat source can be attributed to the high heat capacity of copper [16] and the small volume of the solder droplet.

Light microscopy images were used to measure the intermetallic compound layer thickness in the samples. The 0.5 wt.% Indium samples held at 8 s were selected to illustrate the effect of temperature on the IMC layer thickness. As shown in Fig. 2, the layer at 220 °C looks to be more constant in thickness, while at higher temperatures, a more irregular layer, with more needle-like features resulted. This behavior is similar in all levels of Indium.

The measurement of the intermetallic layer thickness consists in drawing lines perpendicular to the copper surface, as shown in Fig. 3. Measurements were made every 10 μm along the interface in all 10 micrographs, and statistical analysis was done using the Minitab software. Sample sizes ranged from 90 to 120 measurements for a sample, to account for the change in morphology. Figure 4 shows the frequency distributions of the thickness measurements made for each soldering condition. For the 0.5 and 5.0 wt.% In alloys, the thickness data distributions are narrow at the 220 °C level, as compared to the other two temperature levels. This finding supports the fact that at lower temperatures, the intermetallic compound layer growth is relatively uniform, from the interface into the molten

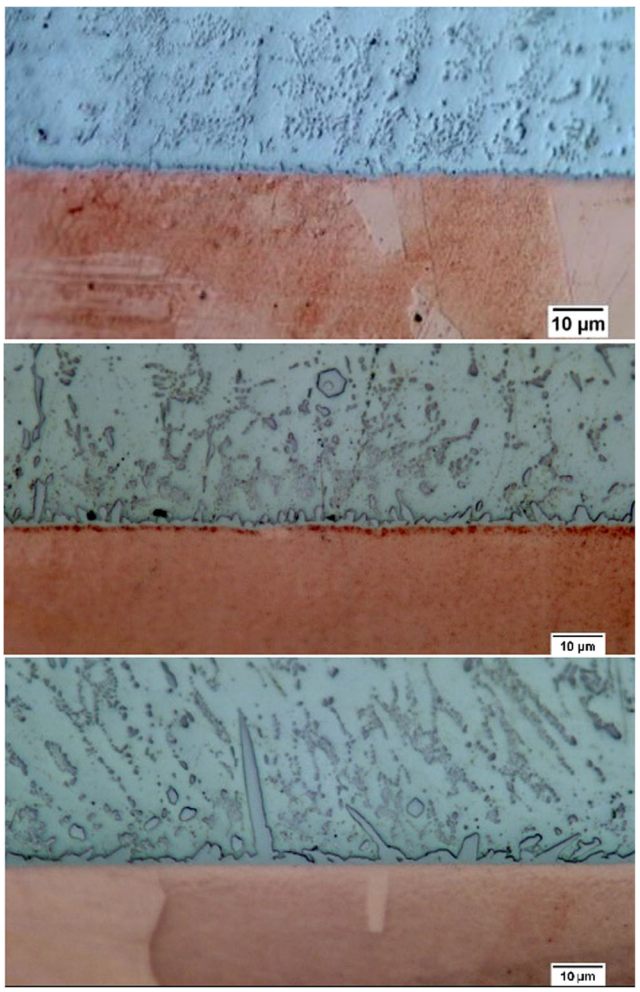

Fig. 2 Comparison of the intermetallic layer in 0.5 wt% Indium solder alloys at increasing hold temperatures from 220 °C (*top*), 275 °C (*center*), to 300 °C (*bottom*). The hold time was 8 s for each condition. Increasing thickness and more needle-like features are observed at higher temperatures

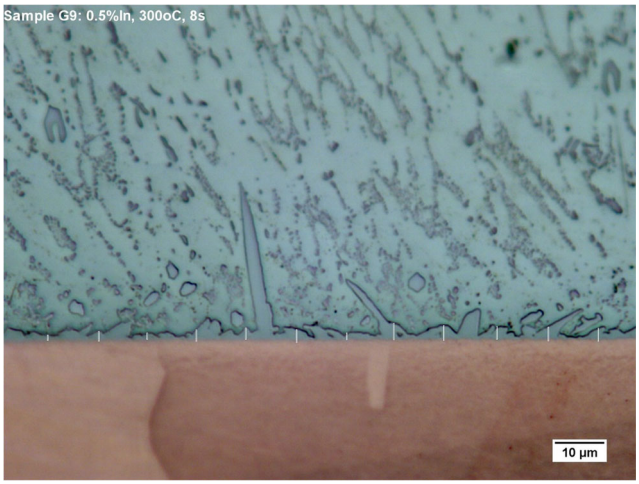

Fig. 3 Procedure to measure the intermetallic compound layer thickness. The *yellow* marks represent the places where the thickness was measured

solder. At higher temperatures, the IMC layers tend to show more needles protruding randomly into the molten solder to cause a larger variability of the data. The relationship between the crystallographic orientation of these needles and the solidification structure of the solder should be investigated with advanced characterization techniques in the future. The distributions observed in Fig. 4 largely support the discussion above.

The mean IMC thicknesses for each sample, as well as their standard deviations, are listed in Table 2 relating time, temperature, and composition of the solder.

For the activation energy calculation, it was considered that the intermetallic compound layer consisted of only one compound. For the SAC305 alloy, the assumption of η-Cu_6Sn_5 as the only product is reasonable; in fact, Cu_3Sn was observed close to the substrate, but its thickness was negligible [7, 8].

Photomicrographs of the 0.5, 5.0, and 10 wt.% Indium samples were taken using the Field Emission Scanning Electron Microscopy (FESEM) in which the presence of the two phases was noticed. All these samples showed the presence of η-Cu_6Sn_5 and Cu_3Sn, but the Cu_3Sn layer located next to the substrate was much smaller than the overall intermetallic compound layer thickness. Thus, the assumption of the layer being composed of just one compound agreed with the literature and is valid for activation energy calculation.

As implied earlier, hold time did not cause any large differences in the interlayer thickness and morphology for the 0.5 and 5.0 wt.% Indium solder alloys. However, for the 10 wt.% Indium alloy, the intermetallic thickness showed considerable changes with time at 220 °C; increasing time increased the amount of IMC. At the higher temperatures of 275 and 300 °C, the IMC thickness did not appear to have changed significantly. The IMC thickness in the 10 wt.% sample appeared to have reached a maximum mean value, for both the 275 and 300 °C temperature. Even at the 220 °C level, the maximum mean thickness was already close to the maximum thickness values achieved at the other temperatures. A possible explanation for the intermetallic compound layer to reach some sort of a maximum value is that Indium allows for an easier intermetallic formation. At higher Indium concentration, a maximum thickness was reached at 2 and 275 °C. Further increase in time or temperature did not result in any

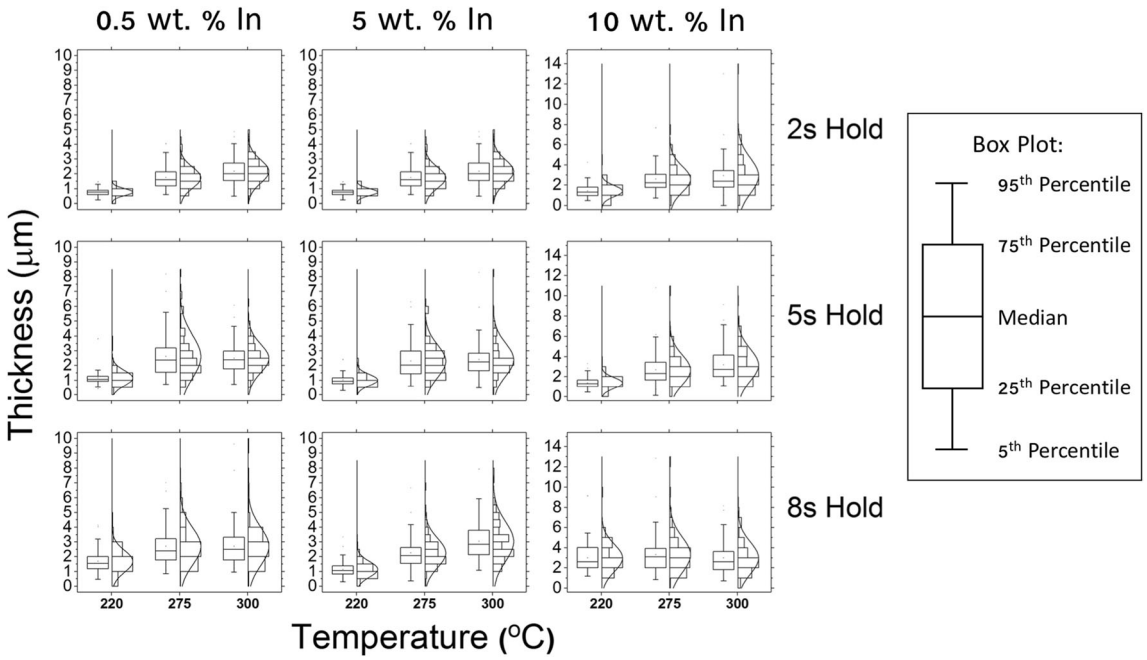

Fig. 4 Frequency distributions of thickness for all solders conditions. Generally, the distribution of thickness measurements widens and skews as the hold temperature is increased. Note the scale on 10 wt.% In

Table 2 The IMC layer mean thickness, standard deviation, and activation energy for each solder condition

Sample	In (wt.%)	Time (s)	Temperature (°C)	Thickness (μm)	SD*	Q(kCal/mol)	Q(eV/atom)
G1	0.5	2	220	1.08	0.50	6.66	0.29
G2	0.5	5	220	1.15	0.51	6.66	0.29
G3	0.5	8	220	1.69	0.73	6.66	0.29
G4	0.5	2	275	2.51	1.36	6.66	0.29
G5	0.5	5	275	2.61	1.44	6.66	0.29
G6	0.5	8	275	2.71	1.26	6.66	0.29
G7	0.5	2	300	2.43	1.25	6.66	0.29
G8	0.5	5	300	2.49	0.97	6.66	0.29
G9	0.5	8	300	2.71	1.30	6.66	0.29
G10	5	2	220	0.76	0.24	5.11	0.22
G11	5	5	220	1.02	0.37	5.11	0.22
G12	5	8	220	1.15	0.52	5.11	0.22
G13	5	2	275	1.75	0.71	5.11	0.22
G14	5	5	275	2.30	1.11	5.11	0.22
G15	5	8	275	2.26	0.99	5.11	0.22
G16	5	2	300	2.17	0.79	5.11	0.22
G17	5	5	300	2.40	1.13	5.11	0.22
G18	5	8	300	3.04	1.35	5.11	0.22
G19	10	2	220	1.41	0.54	10.79	0.47
G20	10	5	220	1.38	0.52	10.79	0.47
G21	10	8	220	2.99	1.36	10.79	0.47
G22	10	2	275	2.59	1.28	10.79	0.47
G23	10	5	275	2.69	1.48	10.79	0.47
G24	10	8	275	3.30	1.75	10.79	0.47
G25	10	2	300	2.93	1.75	10.79	0.47
G26	10	5	300	3.18	1.58	10.79	0.47
G27	10	8	300	2.99	1.59	10.79	0.47

*Thickness measurement standard deviation

major changes. However, at the lower temperature of 220 °C, this maximum value was only reached after 8 s, with increasing thickness with increasing time.

A typical diffusion-controlled behavior as described by eq. 1 below can be assumed for the intermetallic compound growth during solidification [17]. In other words, intermetallic compound layer growth can be described as proportional to the square root of time. In eq. 1,

$$X = (\mathrm{kt})^{\frac{1}{2}} \tag{1}$$

X is the intermetallic compound layer thickness, k is the growth constant and t is the dwell time.

However, in this study many other factors including the liquid metal flow, substrate erosion, and reaction rate between Cu and Sn could have interfered in the IMC growth behavior, in addition to elemental diffusion that could have taken place. Furthermore, for small periods of reaction time like the ones used in this experimental matrix, it may be more appropriate to approximate the IMC growth law using a linear relationship, as described by eq. 2 [5, 6].

$$X = A + \mathrm{kt} \tag{2}$$

In this equation, X is the average IMC thickness, A is the intercept on the X-t plot, k is the growth constant, and t is the time that the solder remains liquid. Figure 5 shows the relation between intermetallic compound layer thickness and time for each of the solder alloys.

The slope (k) of each graph can be related to temperature following the Arrhenius equation, as shown in eq. 3.

$$k = k_0 e^{\frac{-Q}{RT}} \tag{3}$$

where k is the growth rate constant for a giving temperature T, k_o is the pre-exponential constant, Q is the activation energy of the system, and R is the universal gas constant. This equation can be linearized taking natural logarithm of both sides of the equation, as shown in eq. 4.

$$\ln(k) = -\frac{Q}{R}\cdot\frac{1}{T} + \ln(k_0) \tag{4}$$

With this analysis, on a plot relating $1/T$ and $\ln(k)$, the slope of the linear expression from the experimental data is equal to $-\frac{Q}{R}$. The graph relating the inverse temperature and k for the 0.5 wt.% In alloy composition is shown in Fig. 8 to illustrate the activation energy calculation process.

Considering the slope of the graph in Fig. 6 and applying the Arrhenius analysis of the activation energy of the IMC formation and growth was calculated to be 6.7 kCal/mol (0.29 eV/atom) for the 0.5 wt.%. Following a similar procedure, the activation energy for 5 wt.% In alloy was 5.1 kCal/mol (0.22 eV/atom). Finally, for the 10 wt.% of In alloy

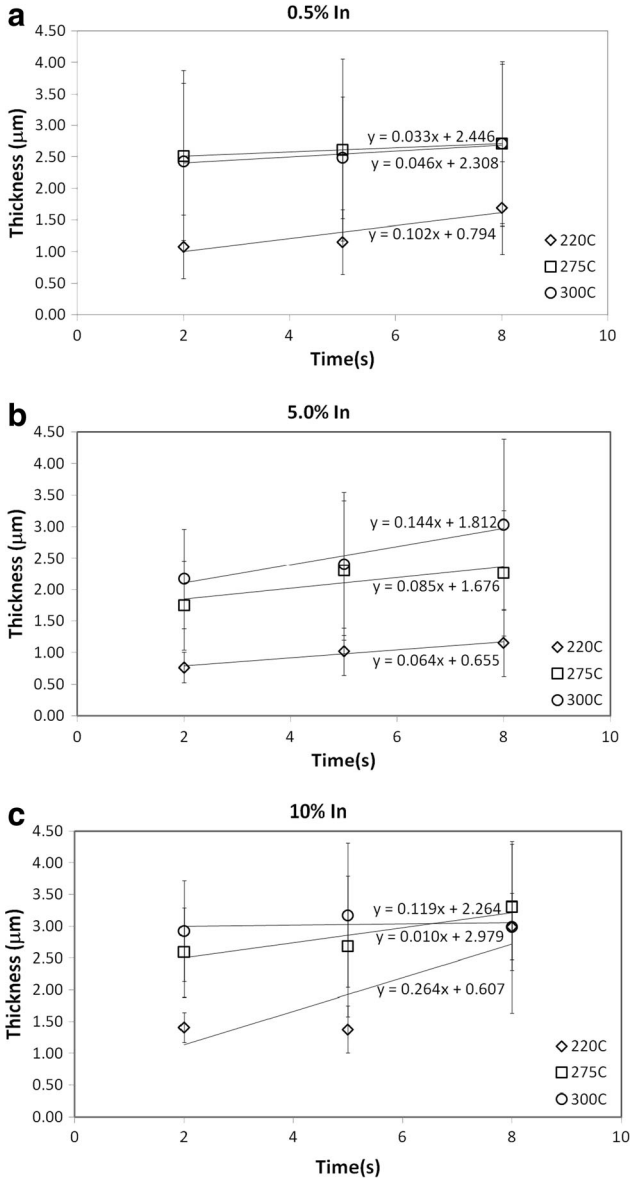

Fig. 5 Relation between time and temperature for all three temperatures in all three alloys. **a** 0.5 wt.% Indium. **b** 5.0 wt.% Indium. **c** 10 wt.% Indium

solder, the activation energy was estimated to be 10.8 kCal/mol (0.47 eV/atom). The degree of uncertainty in these calculations from the thickness, temperature, and time measurements should be evaluated in the future to assess the influence of measurement uncertainties on activation energy determination.

The value of activation energy for the 0.5 wt.% In alloy is smaller than the 8.1 kCal/mol reported by Andrade, Liu and Madeni [8] for SAC305 alloy. The 5.0 wt.% In alloy also showed a comparatively smaller activation energy value. This drop in the activation energy value can be explained by the fact that the addition of Indium decreases the melting point of the alloy [18]. Differential scanning calorimetry tests were performed to evaluate the effect of the addition of indium in

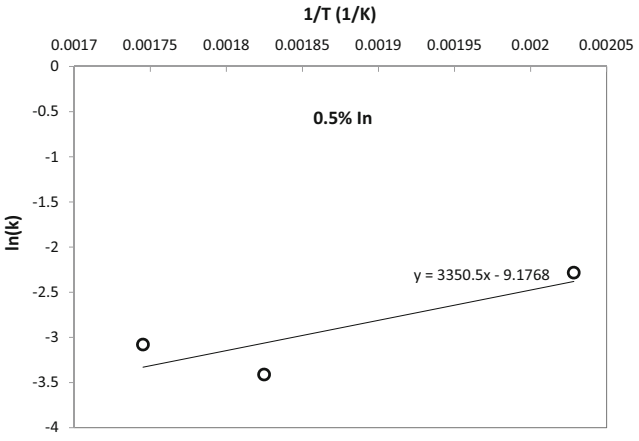

Fig. 6 Relation between ln (K) and $1/T$ used to determine the activation energy of the 0.5 wt.% In alloy system

the melting point of the solder alloy. The melting point of the three solder compositions presented in this work as well as that of the SAC305 reference alloy is summarized in Fig. 7. It is noticeable the decrease in the melting point with the increase of Indium content in the solder composition.

In fact, increasing amount of Indium was also reported to decrease the wetting time, as well as increase the wetting force [19]. These factors would help decrease the activation energy for the formation of the intermetallic compound layer.

However, the activation energy increased to 10.8 kCal/mol in the 10 wt.% In alloy system. Figure 7c shows the relationship between the IMC thickness and time for the three alloys at the three levels of temperature tested. The alloy with the smaller amount of Indium in its composition (0.5 wt.%) showed a better linear fit between IMC thickness and time, while increasing the Indium content gave a worse linear fit.

Note that the activation energy values presented in this paper were obtained assuming that the entire intermetallic compound layer was formed by one single compound. As will be discussed further in this paper, Cu_3Sn was also observed next to Cu_6Sn_5 in the IMC layer, as well as other Indium and Silver

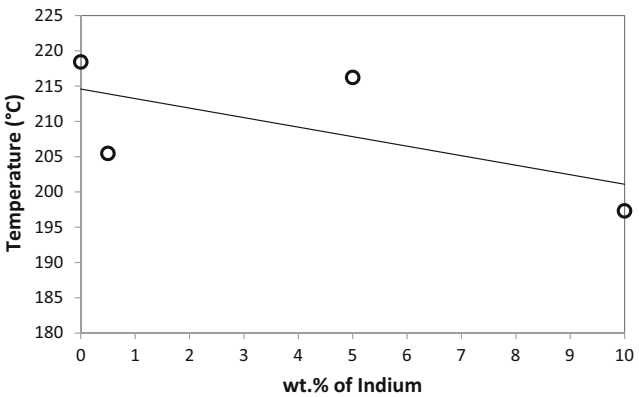

Fig. 7 Relationship between the indium content and the melting point of the alloy

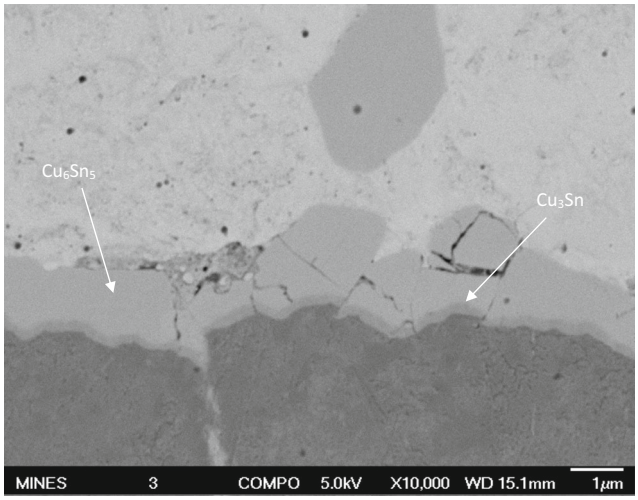

Fig. 8 Electron micrograph of a sample made with the 5.0 wt.%. In solder showing the presence of Cu_6Sn_5 and Cu_3Sn IMC on the copper substrate

containing IMC's. To further identify these compounds, energy dispersive spectroscopy (EDS) measurements were performed on each sample to investigate the presence of other elements in the intermetallic compound layer. The formation of new compounds in the IMC layer can certainly lead to the deviation from the linear relationship of the layer thickness with time. Energy dispersive spectroscopy results showed an increase in the amount of Indium in the intermetallic compound layer with increasing Indium additions. The amounts of Indium found in the layer for the 0.5 and 5.0 wt.% In alloy were considerably low, likely all dissolved in the βSn phase [18, 19]. However, for the 10 wt.% Indium alloys, the amount of Indium found in the intermetallic compound layer was considerably higher. By calculating the atomic percent ratios with the other elements (Cu, Sn, and Ag) found in the layer, it is possible to affirm that the intermetallic compounds formed in these conditions were mostly γ-$InSn_4$ and Cu_6Sn_5. $InSn_4$ has also been reported in the literature in Indium-rich alloys [20, 21].

Field emission scanning electron microscopy (FESEM) was also used to characterize the intermetallic compound layer. As shown in Fig. 8 and in agreement with observations reported in literature [5, 6], Cu_6Sn_5 was found as the principal compound of the intermetallic compound layer. The presence of Cu_3Sn was also noticed close to the copper substrate. The thickness of this layer is considerably thin and should not cause significant changes in the activation energy calculations. The presence of In_4Sn (non-stoichiometric compound with variable Indium ratio) was not noticed due the small acceleration voltage used to get a good quality image, as well as the small atomic number difference between In and Sn. Both intermetallic compounds also exhibit the same hexagonal crystalline structure [2, 22, 23], making it even harder to differentiate between them. For the 10 wt.% In alloy, $InSn_4$ was detected in the bulk of the solder. Ag_3Sn and $AgIn_2$ were also noticed in the solder bulk.

Figure 9 shows the equilibrium binary phase diagram between Tin and Indium, the two major components of the alloy. At room temperature, formation of γ-$InSn_4$ phase is expected for Indium concentrations larger than 7.0 wt.%. Ten weight percent Indium would put the solder composition in a two-phase region, βSn and γ-$InSn_4$. The mixed final microstructure could explain the observed trend of changes in the activation energy and thickness with increasing Indium in the solder alloy.

Finally, cracks were observed in the Cu_6Sn_5 layer, as shown in Fig. 10. Most of the cracks were observed close to

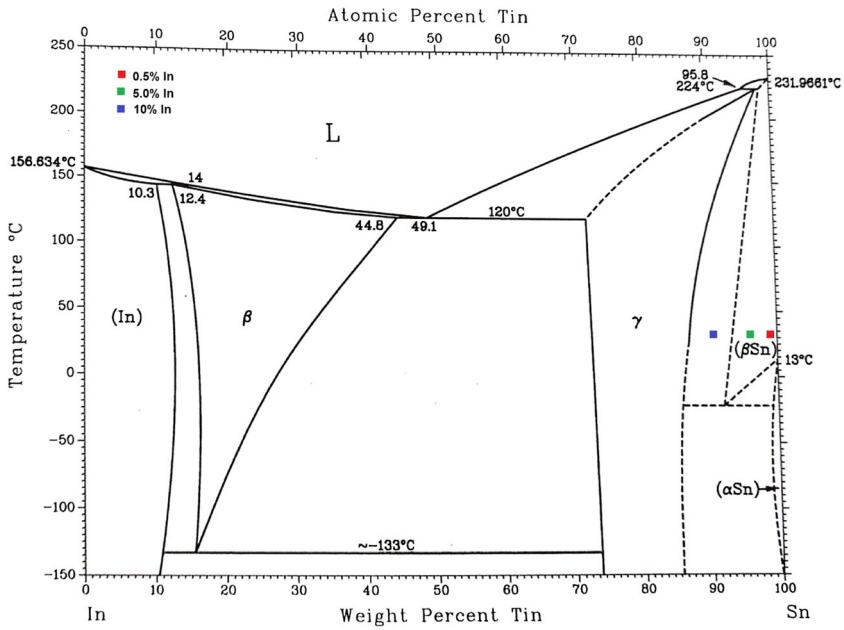

Fig. 9 Equilibrium Sn-In binary phase diagram and alloy location at room temperature [24]

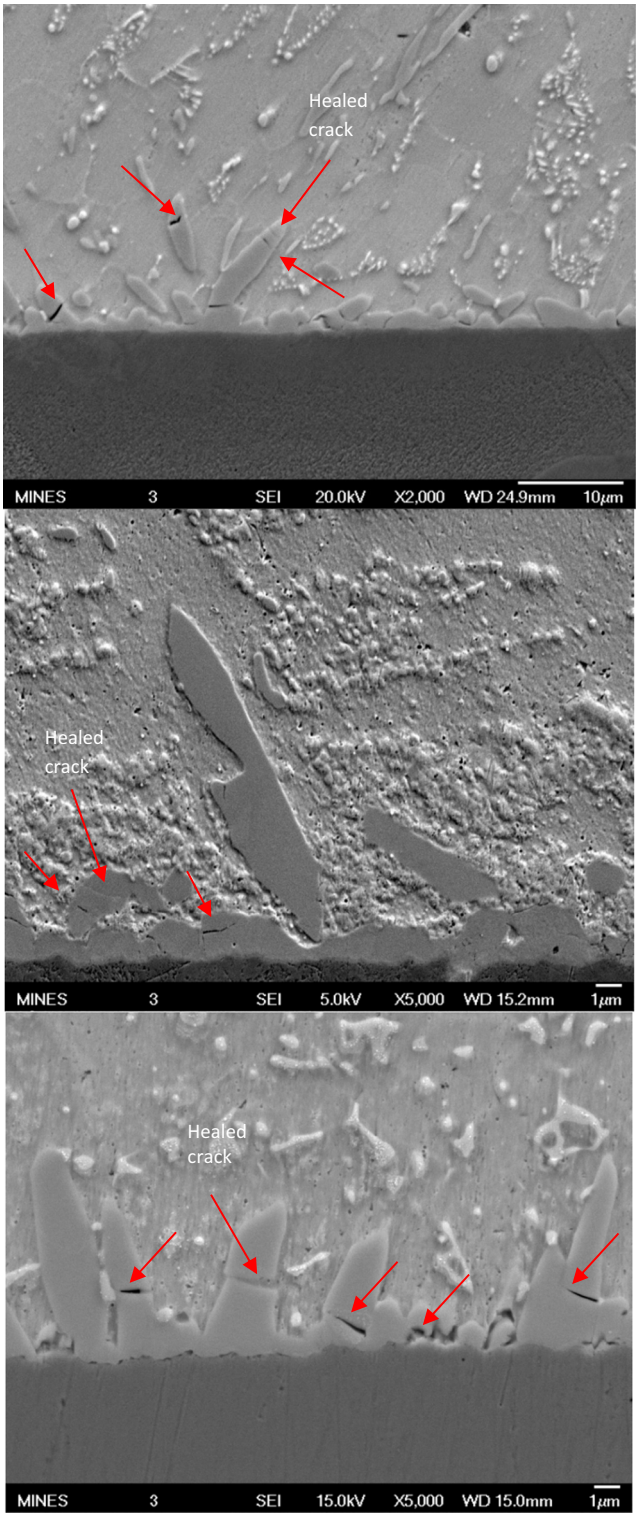

Fig. 10 Comparison between 0.5, 5.0, and 10 wt.% Indium addition levels for the same solder condition. A mixture of cracks and healed cracks are visible. Magnification of 2000X, 5000X, and 5000X, respectively

the solder–substrate interface, at a temperature closer to solidification. Further away from the interface and into the bulk of the solder, crack healing was observed which indicates that cracking occurred when the bulk of the solder was still molten. At a higher temperature, the liquid solder was able to back flow into the crack, and subsequent solidification healed the crack.

4 Conclusions

The present experiments showed that Cu_6Sn_5, Cu_3Sn, In_4Sn (β), $InSn_4$ (γ), Ag_3Sn, and $AgIn_2$ intermetallic compounds were formed. The IMC layer also grew while in the liquid state, similar to what was observed in the commercial SAC305 alloy by Andrade, Liu, and Madeni [5]. Cu_6Sn_5 was identified in the intermetallic compound layer next to the solder/copper interface. The presence of $InSn_4$ was also identified in the 10 wt.% In solder alloy. The activation energy for the formation of the intermetallic compounds for the 0.5 and 5.0 wt.% In solders was smaller, 6.7 and 5.1 kCal/mol, respectively, than the 8.1 kCal/mol for the commercial SAC305 alloy. In the 10 wt.% In solder, an increase in the activation energy to 10.8 kCal/mol was observed. This increase can be explained by the formation of a γ- $InSn_4$ phase. Additionally, the IMC was formed in a βSn matrix with increasing Indium composition in the solder alloy. It was also noticed the formation of In_4Sn in the intermetallic compound layer, further contributing to the changes observed in the calculation of the activation energy.

Acknowledgements The authors acknowledge the support of the Center for Welding, Joining, and Coatings Research for the completion of this research. One of the authors (FR) acknowledges the Brazilian Scientific Mobility Program for their support while interning at the Colorado School of Mines.

References

1. Tong S, von Schirnding YE, Prapamontol T (2000) Environmental lead exposure: a public health problem of global dimensions. Bull World Health Organ 78(9):1068–1077
2. Abtew M, Selvaduray G (2000) Lead-free solders in microelectronics. Mater Sci Eng 27:95–141
3. Siewert TA, Madeni JC, Liu S et al. (2002) Database for solder properties with emphasis on new lead-free solders", National Institute of Standards and Technology & Colorado School of Mines, http://www.msed.nist.gov/solder/NIST_LeadfreeSolder_v4.pdf.
4. Trumble B (1998) Get the lead out! [lead free solder]. Published in the IEEE Spectrum 35(5):55–60
5. Madeni JC, Liu S, Andrade PHS, Carson CH (2015) Characterization and growth kinetics of the formation of intermetallic compounds in the liquid state during soldering with lead-free solders. Published in the IIW Welding in The World Journal 59(3): 325–338 . doi:10.1007/s40194-014-0202-3, ISSN 0043-2288Published online
6. Fallahi H, Nurulakmal MS, Fallahi A, Abdullah J (2012) Modifying the mechanical properties of lead-free solder by adding

iron and indium and using a lap joint test. Published in the Journal of Mater Science: Mater Electron 23(9):1739–17492
7. Hodulova E (2016) Common bilateral joining project Slovakia–Portugal, presented at the 69th IIW Annual Assembly in Melbourne, Australia, and published as IIW Doc XVII-0040-16, July 11–15
8. Andrade PHS, Liu S, Madeni JC (2015) Characterization of Intermetallic Compound Formation and Growth Kinetics in Lead-Free Solder SAC305, presented in International Brazing & Soldering Conference 2015 (IBSC 2015), American Welding Society
9. Yazzie KE, Xie HX, Williams JJ, Chawla N (2012) On the relationship between solder-controlled and intermetallic compound (IMC)-controlled fracture in Sn-based solder joints. Scr Mater 66:586–589. doi:10.1016/j.scriptamat.2012.01.009
10. Salam B, Ekere NN, Rajkumar D (2001) Study of the interface microstructure of Sn-Ag-Cu lead-free solders and the effect of solder volume on intermetallic layer formation. Published in the Electronic Components and Technology Conference, 2001. Proceedings., 51st, pp. 471–477. doi: 10.1109/ECTC.2001.927769
11. Pecht M (1993) Soldering processes and equipment. Wiley, New York
12. Tu PL, Chan YC, Lai JKL (1997) Effect of intermetallic compounds on the thermal fatigue of surface mount solder joints. Published in IEEE Transactions on Components, Packaging, and Manufacturing Technology: Part B 20(1):87–93. doi:10.1109/96.554534
13. Parent JOG, Chung DDL, Bernstein IM (1988) Effects of intermetallic formation at the interface between copper and lead-tin solder. J Mater Sci 23:2564. doi:10.1007/BF01111916
14. Li M, Du Z, Guo C, Li C (2009) Thermodynamic optimization of the Cu–Sn and Cu–Nb–Sn systems. J Alloys Compd 477:104–117
15. Biocca P (2006) Tin-copper based solder options for lead-free assembly. Global SMT & Packaging - November/December
16. White GK and Collocott SJ (1984) Heat capacity of reference materials: Cu and W. J Phys Chem Ref Data. 13(4)
17. Siewert TA, Madeni JC, and Liu S (2003) Formation and growth of intermetallics at the interface between lead-free solders and copper substrates. Proceedings of the APEX Conference on Electronics Manufacturing, Anaheim, California
18. YEH MS (2003) Effects of indium on the mechanical properties of ternary Sn–In–Ag solders. Metall Mater Trans A 34A:361–365
19. Kanlayasiri K, Mongkolwongrojn M, Ariga T (2009) Influence of indium addition on characteristics of Sn-0.3Ag-0.7Cu solder alloy. J Alloys Compd 485:225–230
20. Ohnuma I, Cui Y, Liu XJ, Inohana Y, Ishihara S, Ohtani H, Kainuma R, Ishida K (2000) Phase Equilibria of Sn-in based micro-soldering alloys. J Electron Mater 29(10):1113–1121
21. Liu XJ, Inohana Y, Takaku Y, Ohnuma I, Kainuma R, Ishida K, Moser Z, Gasior W, Pstrus J (2002) Experimental determination and thermodynamic calculation of the phase Equilibria and surface tension in the Sn-Ag-in system. J Electron Mater 31(11):1139–1151
22. Zhao Y, Zhang Z, Dang H (2004) Synthesis of In-Sn alloy nanoparticles by solution dispersion method. Journal of Material Chemistry 14:299–302
23. Mu D, Huang H, McDonald SD, Read J, Nogita K (2013) Investigating the mechanical properties, creep and crack pattern of Cu_6Sn_5 and $(Cu,Ni)_6Sn_5$ on diverse crystal planes. Materials Science and Engineering: A, Volume 566(20):126–133
24. Jacobson DM and Humpston G (2004) Principles of Soldering. ASM International, The Materials Information Society